Optimization of the synthesis parameters to obtain Mo_2TiAlC_2 MAX phase

A

Thesis

Submitted in partial fulfillment of the

requirements for the award of the degree of

MASTER OF SCIENCE

by

Jaspreet Kaur

(301604018)

Under the Supervision of

Dr. O.P. Pandey

(Senior Professor & Head)

School of Physics & Materials Science

Thapar Institute of Engineering and Technology (TIET), Patiala - 147004

July 2018

CERTIFICATE

This is to certify that the thesis entitled **'Optimization of the synthesis parameters to obtain Mo_2TiAlC_2 MAX phase'** submitted by **Jaspreet Kaur** (Roll no: 301604018) for the fulfilment of the requirement for the award of degree of Master in Physics, Thapar Institute of Engineering and Technology, Patiala (Punjab), India. It is an exclusive record of candidate's own research under the supervision of Dr. O. P. Pandey. This dissertation in part or full has not been submitted in any other institution for the award of such kind of degree.

Dr. O.P. Pandey
(Supervisor)
Senior Professor
School of Physics and Materials Science
Thapar Institute of Engineering and Technology, Patiala

DECLARATION

I hereby declare that work been presented in this thesis report entitled **'Optimization of the synthesis parameters to obtain Mo_2TiAlC_2 MAX phase'** by me in partial fulfilment of the requirements for the award of degree of Master of Science in Physics, Thapar Institute of Engineering and Technology, Patiala is authentic award record on my work carried out under the supervision of Dr. O. P. Pandey (Senior Professor), School of Physics and Materials Science, Thapar Institute of Engineering and Technology, Patiala. The matter in the report has not submitted by any other university/Institute for the award of master and science or any other degree.

Jaspreet Kaur

Jaspreet Kaur

301604018

ACKNOWLEDGMENT

First and Foremost. I would like to express my deep sense of gratitude and respect to my supervisor **Dr. O.P. Pandey** Senior Professor & Head of Department (School of Physics and Materials Science) for his valuable discussions, strong motivation, guidance and encouragement during the course of the work. Secondly, I would like to thank **Mr. Piyush Sharma** for guiding me throughout this dissertation. I am grateful to my co-mentor for enlightening me the first glance of research.

I express to the deepest gratitude to the senior most Post-Doc. **Dr. Gurbinder Kaur** and Ph.D. Scholars **Mr. Aayush Gupta, Mr. Rameez Ahmad Mir, Ms. Ruby Priya, Ms. Raveena, Ms. Shivani Bansal, Mrs. Suninder Kaur and Ms. Damandeep Kaur** for their moral support and constant co-operation whenever required.

I would also like to thank my colleagues **Ms. Navpreet Kaur** and **Ms. Neha Rani** for their support during my project work.

I am privileged for having best friends **Ms. Kaveri** and **Ms. Gaganjot** who provided continuous support and help during the complete journey.

The meaning of life is incomplete without paying regards to my parents **Mr. Harnam Singh Bedi** and **Mrs. Pushpinder Kaur** who have constantly helped me to keep my morale high throughout the research work. I also thank my brother **Mr. Harjeet Singh Bedi** for guiding me at every stage of my life.

Jaspreet Kaur.

Jaspreet Kaur

(301604018)

ABSTRACT

Transition metal carbides (TMC's) emerged as an important class of materials for wide range of industrial applications. The wide applicability of a TMC's is limited due to their brittle nature. To enhance the ductility of TMC's, a metallic character has to be introduced. This lead to development of novel class of materials known as MAX phases. These are nano-laminated ternary compounds possess remarkable combination of both metallic and ceramic properties such as high stiffness, high electrical conductivity, thermally stable and low thermal coefficients. Herein, the synthesis of the Mo_2TiAlC_2 MAX phase via conventional sintering method is investigated. The sintering parameters are optimized to obtain Mo_2TiAlC_2 MAX phase. The role of titanium carbide precursor for the synthesis of Mo_2TiAlC_2 MAX phase is studied. The structural properties of the prepared samples are studied through X-Ray Diffraction Technique. Also, the morphology of the prepared sample is studied via Scanning Electron Microscopy (SEM).

LIST OF FIGURES

LIST OF TABLES

TABLE OF CONTENTS

CHAPTER 1

INTRODUCTION

1.1. Introduction

Transition metal carbides (TMC's) emerged as important class of materials for industrial applications. These materials exhibit unique physical properties such as high melting point, high hardness value, high electronic conductivity, and good corrosion resistant [1, 2]. However, the wide applicability of a TMC's limits due to their brittle nature. So, to enhance the ductility of TMC's, metallic character has been introduced in it [3]. This has led to the development of novel class of materials known as MAX phases. These ternary ceramics possess general formula $M_{n+1}AX_n$ (n = 1,2,3…), where M is transition metal, A is 13 to 16 group elements in the periodic table, and X is carbon and/or nitrogen [4]. In MAX phases, the M-X bonds are metallic-covalent in nature, which are relatively strong together with M-A bond that is relatively weak.

MAX phases are firstly discovered by Nowotny and his co-workers in 1960's [5]. These phases were initially called as H-Phases and their relatives are Ti_3SiC_2 and Ti_3GeC_2. Later in 2000, Barsoum and co-workers named these compounds as MAX phases [6]. According to literature, there are total 10 elements in the periodic table which are considered as M elements and 12 A elements as shown in figure 1.1.

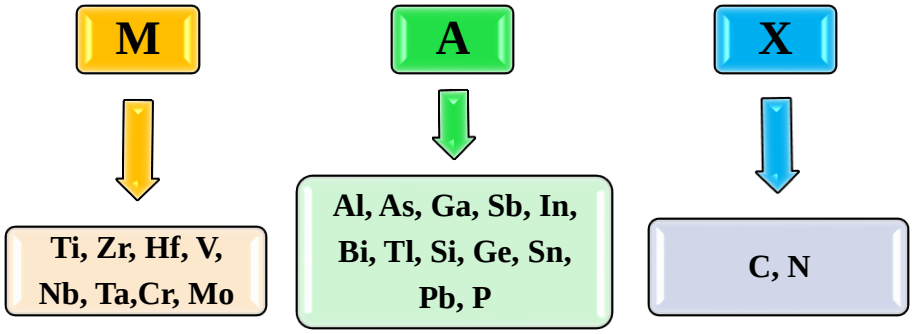

Fig. 1.1 Representation of M, A and X elements.

MAX phases possess remarkable combination of both metallic and ceramic properties such as high stiffness, high electrical conductivity, thermally stable and low thermal coefficients. These phases are polycrystalline solid that normally deform by a combination of kink band and shear band formation together with delamination of individual grains [7]. In these phases, dislocations multiply and are mobile at room temperature, glide exclusively on the basal planes, and arranged in arrays or kink boundaries. Therefore, MAX phases are easily machinable and exhibit very decent mechanical properties, especially at temperatures below 1000 ºC [8]. Due to all these unique properties MAX phases are used for elevated temperature structural applications, wear and corrosion protection, heat exchangers and for low friction applications based on basal plane lubricity [9].

1.2. Molybdenum based MAX phases

Among all the known MAX phases, molybdenum (Mo) based MAX phases are the least studied, even though molybdenum (Mo) has high mechanical strength and hardness at elevated temperature [14]. Recently, a double-layered Mo-containing ordered MAX phase has been synthesized, i.e. $Mo_2TiAlC_2$and $Mo_2Ti_2AlC_3$ in which molybdenum (Mo) is doped with $Ti_3AlC_2$and Ti_4AlC_3 ternary compounds [15]. In these MAX phases, Ti atoms are sandwiched between two Mo layers and these Mo layers are bonded with Al layers to form Mo-Ti-Mo-Al-Mo-Ti-Mo and Mo-Ti-Ti-Mo-Al-Mo-Ti-Ti-Mo stacking order [16]. However, the detailed synthesis and the synthesis mechanism is not studied. So, it is crucial to understand the detailed synthesis mechanism involved during the synthesis of double layered MAX phases.

1.3. Crystal structure

More than 90 MAX phases of different chemical compositions share a common hexagonal structure with $P6_3/mm$ symmetry [10]. In these compounds, M layer is intercalated with single A layer, having X in the octahedral sites. The M_6X octahedral with X atoms filling the octahedra sites between M atoms, which are identical to those of rock salt structure of MX binaries [11]. The octahedra alternate with A layers elements located at the centre of trigonal prisms that are slightly larger and thus able to accommodate the larger A atoms [12]. Fig.1.2 shows the unit cells of MAX phases M_2AX (211), M_3AX_2 (312), M_4AX_3 (413). In 211 MAX phases, two layers of M separate A layer. Similarly, in 312 and 413 MAX phases, A layers are separated by three and four M layers respectively [13].

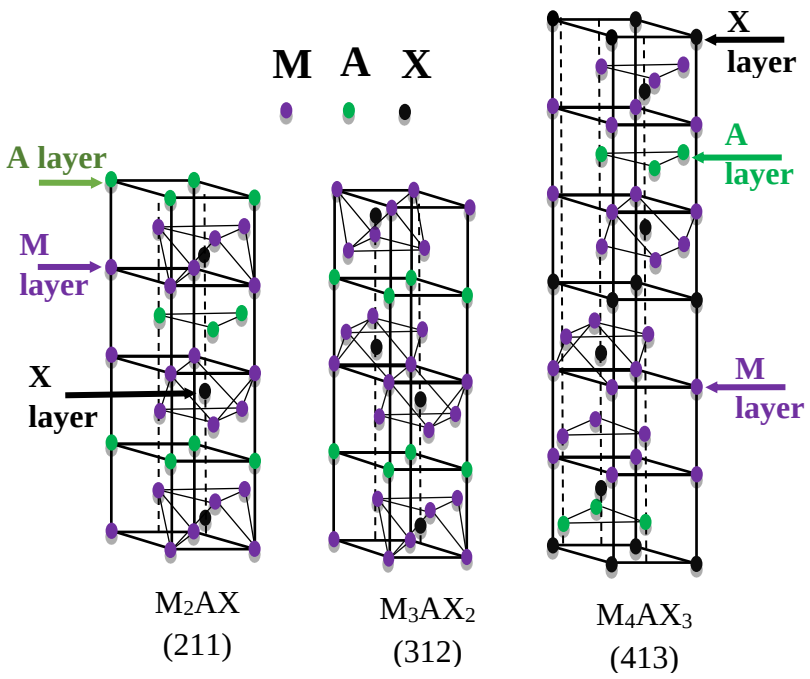

Fig. 1.2 Unit cells of MAX phases M_2AX (211), M_3AX_2 (312), M_4AX_3 (413).

1.4. Synthesis methods

Numerous synthesis methods have been reported for the synthesis of MAX phases. MAX phases can be synthesised in the form of thin film, thick film and bulk. Thin film of MAX phases can be prepared through physical vapour deposition (PVD) and chemical vapour deposition (CVD) methods. The bulk MAX phases can be synthesised through sintering process. The brief description of the synthesis of MAX phases is as follows:

1.4.1. Physical Vapor Deposition (PVD)

In this process, deposition occurs through the vaporization of a solid or liquid material in a vacuum chamber. The vapours in the form of atoms or molecules are transported to the substrate, where it gets condensed [17]. The thickness of the MAX phase films prepared through this method can be varied from few nanometres to thousand nanometres. PVD can also be used for the synthesis of multilayer coatings, graded composition, thick deposition, and self-supporting structures [18]. The magnetic sputtering system is commonly used for the physical vapor deposition. The schematic representation of the magnetic sputtering system is presented in Fig 1.3.

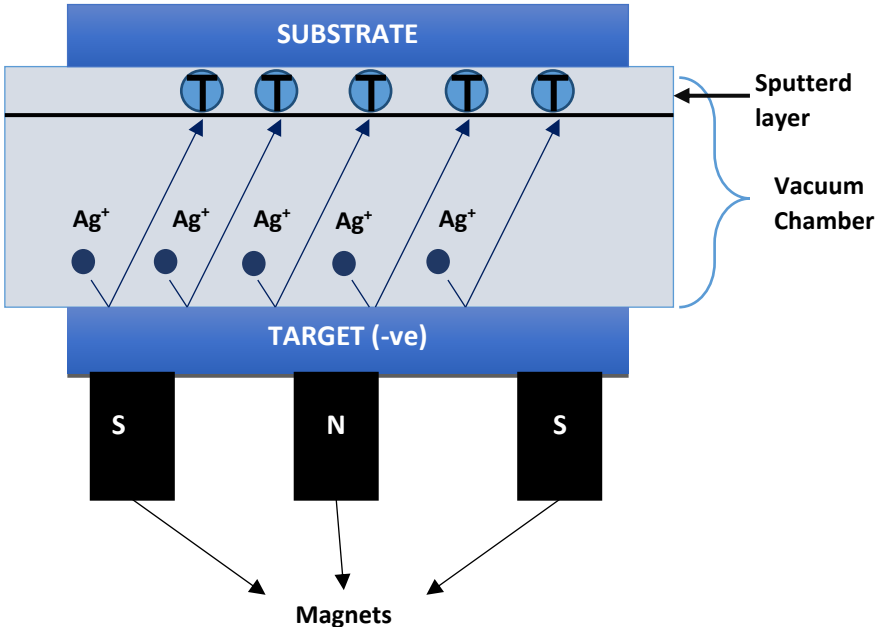

Fig. 1.3 Schematic diagram of magnetic sputtering system.

1.4.2. Chemical Vapour Deposition (CVD)

Chemical vapour deposition (CVD) process involves a chemical reaction through which a solid or liquid material is deposited over the surface of substrate [19]. In this case, reduction or decomposition of the chemical vapor precursor occurs to form a new compound. In addition, plasmas can be used in CVD process to initiate the reaction between the precursors

[20]. MAX phases thin films prepared through CVD possess very low porosity and excellent surface coverage. Figure 1.4 shows the schematic diagram of chemical vapour deposition.

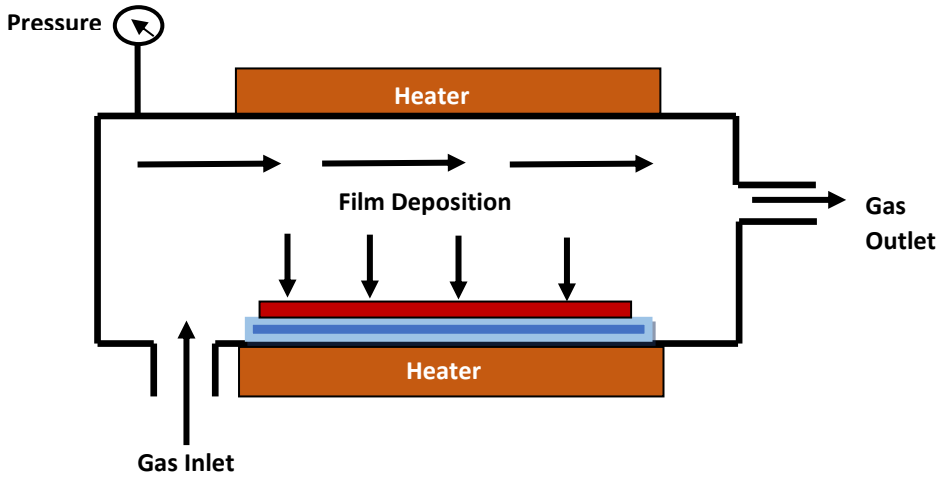

Fig. 1.4 Schematic diagram of chemical vapour deposition.

1.4.3. Sintering process

Sintering is the heat treatment process that involves compacting of powder into a solid material [21]. Initially, the powder is cold pressed and then heat treated at desired temperature. The driving force involved during sintering process is the reduction of the surface energy. The heat treatment reduces the surface area through the formation of bonds between the particles. Sintering process also reduces the porosity and enhances the ductility, strength and hardness of the material [22]. The heating treatment is provided under the controlled temperature. In case of the MAX phase, the sintering is performed in an inert atmosphere to avoid oxidation. In general, sintering occurs in three steps: (a) Necking of the grains, (b) The growth of necking of the grains followed by elimination of pores and (c) The pores get isolated shown in figure 1.5 [23].

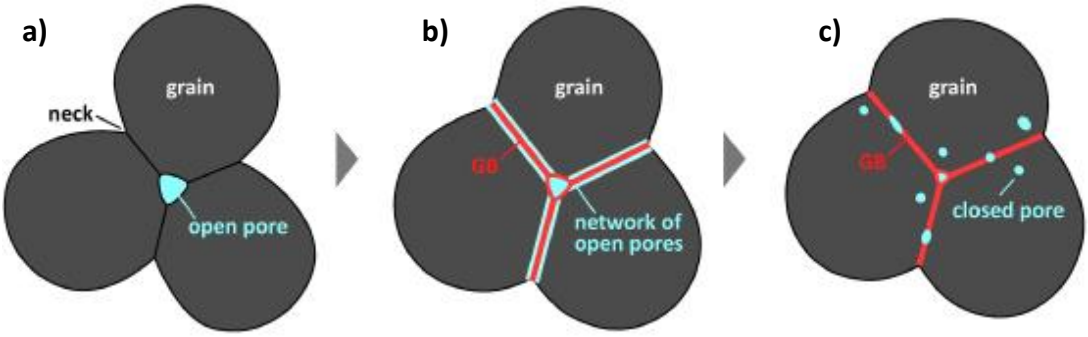

Fig. 1.5 Steps of sintering process a) Necking of grains. (b) The necks and grain boundaries grown followed by elimination of pores. (c) The pores get isolated [23].

There are mainly four types of sintering processes are used to prepare MAX phases i.e. conventional sintering, hot pressing (HP), hot isostatic pressing (HIP) and spark plasma sintering (SPS) [24]. In the conventional sintering, no mechanical pressure is induced on the material during the heat treatment. However, in hot pressing (HP) and hot isostatic pressing (HIP) sintering, the mechanical pressure is induced on the powder material under heat treatment [25]. In order to prevent oxidation of the MAX phases, HP and HIP is performed in vacuum or inert gas atmosphere [26]. The major advantage of HP and HIP methods is the combination of mechanical pressure and heat treatment that results into good densification and reduces the number of structural defects. Figure 1.6 shows the schematic diagram of hot pressing (HP) process.

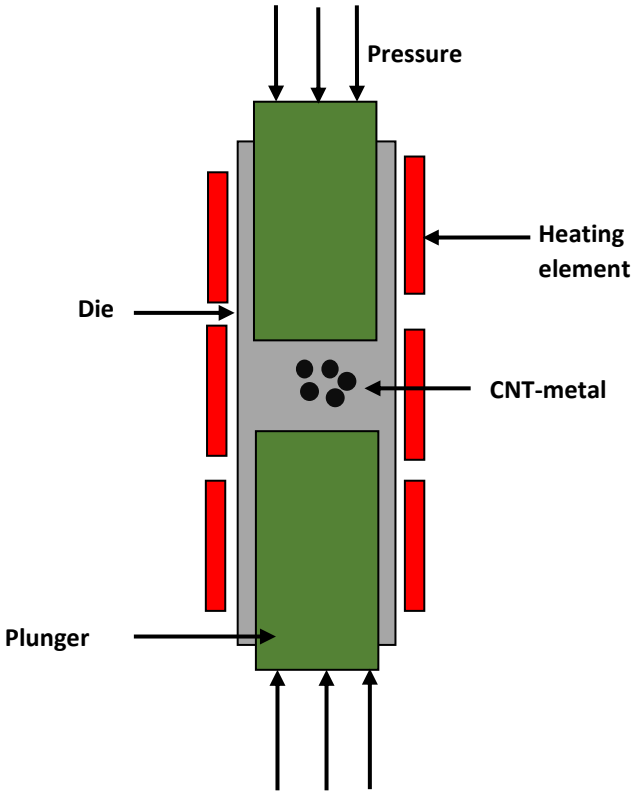

Fig. 1.6 Schematic diagram of hot pressing (HP) process.

In spark plasma sintering (SPS) technique, a direct electric current is applied to heat up the electrically conductive devices through graphite die under low atmospheric pressure [27]. The powder is compacted by joule heating. This process was developed on the idea of using plasma on electric discharge machine for sintering metals and ceramics [28]. There are various names of spark plasma sintering such as plasma activated sintering, plasma electric current sintering and electric current-activated sintering. In this method, electric current and mechanical pressure is applied side by side for solidification and densification [29]. Figure 1.7 represents the schematic diagram of spark plasma sintering.

1.5. Applications of MAX phases

MAX phases are used in wide applications because of its unique properties. The properties such as low friction, good thermal and electrical conductors, good machinability makes them attractive heating elements, gas burning applications, heat exchangers etc [12].

1.5.1. Elevated Temperature Applications

Graphite is refractory compound finding potential application in industries. This material is a used for the hot pressing of diamond-cutting tools. Instead of graphite, MAX phases have better wear and oxidation resistance. Moreover, MAX phases can be machined easily due to high tolerance.

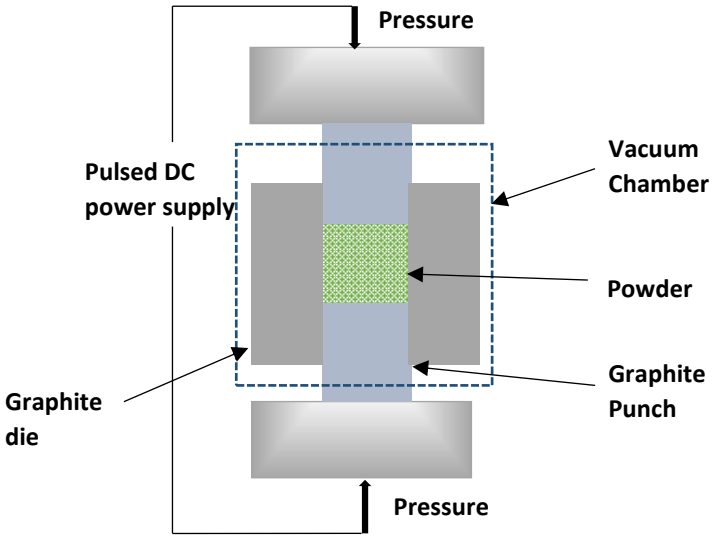

Fig. 1.7 Schematic diagram of spark plasma sintering.

1.5.2. Gas Burning Applications

MAX phases are widely used in gas burning applications. Due to its high-temperature properties it forms a protective Al_2O_3 layer. For example, Mo_2TiAlC_2-based MAX phases are used in gas burner nozzles. Figure 1.8 shows the Ti_2AlC in comparison to steel nozzles used in gas burners. The burner process temperature can be increased upto 1400^0C when MAX phase compounds are used instead of metallic alloys.

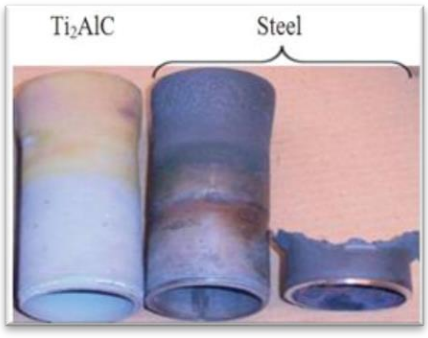

Fig. 1.8 Ti_2AlC steel nozzles used in gas burners [12].

1.5.3. Heating Elements

MAX phase has found various application in heating elements. The heating elements are made from different MAX phases and can be heated up to 1350 ^{0}C, cooled down to room temperature for ≈10 000 cycles. Figure1.9 shows the Ti_2AlC heating element is heated at 1450^{0}C.

Fig. 1.9 Ti_2AlC MAX phase heating element [6].

1.5.4. Application in Nuclear Industry

Cladding materials are coated with MAX phases to protect them from oxidation. Cladding oxidation causes mechanical failure and leave the nuclear fuel unprotected which leads to the fission of the product formed [30]. Therefore, it is important to coat the material with high oxidation resistant at elevated temperature. The cladding materials such as zircolay tube is used to hold the nuclear fuel. To coat Zircolay tubes thin layer of MAX phase (Ti_2AlC or Ti_3AlC_2) is sprayed on them. This thin layer of alumina protects the Zircolay tubes from the coolant losses.

1.5.5. Foil bearings

The Ag-based MAX composites are used for foil bearing applications having low friction. The bearings such manufactured undergo high rotations, while the loads are low. Moreover, these foil bearings are capable to work at ambient as well as elevated temperatures. Figure1.10 (a) shows the Ag/Ta_2AlC composites cylinder and (b) super alloy foil. Further, these composites undergo rigorous rig testing, where parts revolved at 50000 revolutions per minute [16].

a) **b)**

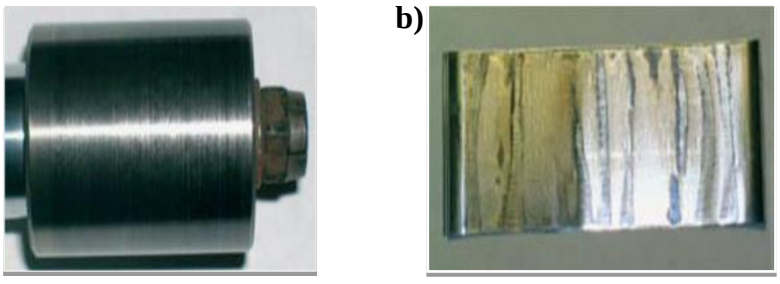

Fig. 1.10 (a) Ag/Ta_2AlC composites cylinder. (b) Super alloy foil [16].

References

[1] C. Kral, W. Lengauer, D. Rafaja, and P. Ettmayer, Critical Review on the Elastic Properties of Transition Metal Carbides, Nitrides and Carbonitrides. *ChemInform*, 29(2010) 215-233.

[2] J. Wang and Y. Zhou, Recent Progress in Theoretical Prediction, Preparation, and Characterization of Layered Ternary Transition-Metal Carbides, 39(2009) 415-443.

[3] Y. Xiao, J.-Y. Hwang, and Y.-K. Sun, Transition metal carbide-based materials: synthesis and applications in electrochemical energy storage. *J. Mater. Chem. A*, 4(2016) 10379–10393.

[4] D. T. Cuskelly, E. H. Kisi, and H. O. Sugo, MAX phase – Alumina composites via exchange reaction in the $M_{n+1}AlC_n$ systems (M=Ti, V, Cr, Nb, or Ta). *J. Solid State Chem.* 233(2016) 150–157.

[5] M. W. Barsoum, The $M_{N+1}AX_N$ Phases : A New Class of Solids. *Prog. Solid State Chem.* 28(2000) 201–281.

[6] B. M. Radovic and M. W. Barsoum, MAX phases : Bridging the gap between metal and ceramics. *Am. Ceram. Soc. Bull.* 92(2013) 20–27.

[7] M. W. Barsoum and M. Radovic, Elastic and Mechanical Properties of the MAX Phases. *Annu. Rev. Mater. Res.*41(2011) 195–227.

[8] M. W. Barsoum, L. Farber, and T. El-Raghy, Dislocations, kink bands, and room-temperature plasticity of Ti_3SiC_2. *Metall. Mater. Trans.* 30(1999) 1727–1738.

[9] M. F. Cover, O. Warschkow, M. M. M. Bilek and D. R. McKenzie, Elastic properties of $Ti_{n+1}AlC_n$ and $Ti_{n+1}AlN_n$ MAX phases, *Adv. Eng. Mater.* 10(2008) 935–938.

[10] Z. Liu, E. Wu, J. Wang, Y. Qian, H. Xiang, X. Li, Q. Jin, G. Sun, X. Chen, J. Wang and M. Li, Crystal structure and formation mechanism of $(Cr_{2/3}Ti_{1/3})_3AlC_2$ MAX phase. *Acta Mater.* 73(2014) 186–193.

[11] Z. M. Sun, Progress in research and development on MAX phases: a family of layered ternary compounds, *Int. Mater. Rev.* 56(2011) 143–166.

[12] M. Atikur Rahman, Study on Structural, Electronic, Optical and Mechanical Properties of MAX Phase Compounds and Applications. *Am. J. Mod. Phys.* 4(2015) 75.

[13] P. Eklund, J. Rosen, and P. O. Å. Persson, Layered ternary $M_{n+1}AX_n$ phases and their 2D derivative MXene: An overview from a thin-film perspective. *J. Phys. D. Appl. Phys.* 50(2017) 113001.

[14] M. Sortino, G. Totis, and F. Prosperi, Dry turning of sintered molybdenum. *J. Mater. Process. Technol.* 213(2013) 1179–1190.

[15] B. Anasori, M. Dahlqvist, J. Halim, E. J. Moon, J. Lu, B. C. Hosler, El'ad N. Caspi, S. J. May, L. Hultman, Per Eklund, J. Rosen and M. W. Barsoum, Experimental and theoretical characterization of ordered MAX phases Mo_2TiAlC_2 and $Mo_2Ti_2AlC_3$. *J. Appl. Phys.* 118(2015) 094304.

[16] B. Anasori, J. Halim, J. Lu, C. A. Voigt, L. Hultman, and M. W. Barsoum, Mo_2TiAlC_2: A new ordered layered ternary carbide. *Scr. Mater.*, vol. 101, pp. 5–7, 2015.

[17] D.M. Mattox, Handbook of Physical Vapour Deposition (PVD) processing, *Elsevier*, 2nd edition, (2010) 792.

[18] N. Selvakumar and H. C. Barshilia, Review of physical vapor deposited (PVD) spectrally selective coatings for mid- and high-temperature solar thermal applications. *Sol. Energy Mater. Sol. Cells*. 98(2012) 1–23.

[19] H.O.Pierson, Fundamentals of Chemical Vapor Deposition, Elsevier 2nd edition,(1999) 458.

[20] Q Q. Zhang, D. Sando, and V. Nagarajan, Chemical route derived bismuth ferrite thin films and nanomaterials, *J. Mater. Chem. C*, 4(2016) 4092–4124.

[21] Suk-Joong L.Kang, Sintering Densification,Grain Growth,and Microstructure, *Elsevier* (2005) 9–18.

[22] X. Jiao, X. Wang, P. Feng, Y. Liu, L. Zhang, and F. Akhtar, Microstructure Evolution and Pore Formation Mechanism of Porous $TiAl_3$ Intermetallics via Reactive Sintering, *Acta Metall. Sin.*2017.

[23] H. Tanaka, A. Yamamoto, J. I. Shimoyama, H. Ogino, and K. Kishio, Strongly connected exsitu MgB_2 polycrystalline bulks fabricated by solid-state self-sintering. *Supercond. Sci. Technol.* 25(2012) 11.

[24] L. A. Dobrzański, A. D. Dobrzańska-Danikiewicz, A. Achtelik-Franczak, L. B. Dobrzański, E. Hajduczek, and G. Matula, Fabrication Technologies of the Sintered Materials Including Materials for Medical and Dental Application. (2017) 17–52.

[25] K. S. Munir, P. Kingshott, and C. Wen, Carbon Nanotube Reinforced Titanium Metal Matrix Composites Prepared by Powder Metallurgy—A Review. *Solid State Mater. Sci.* 40(2015) 38–55.

[26] M.P. Groover, Fundamental of modern manufacture materials, process and synthesis. *Wiley Publications* 1(2012) 386-390.

[27] N. C. Ghosh and S. P. Harimkar, Consolidation and synthesis of MAX phases by spark plasma sintering (SPS): A review. *Woodhead Publishing Limited* 2012.

[28] Z. Shen, M. Johnsson, Z. Zhao, and M. Nygren, Spark plasma sintering of alumina. *J. Am. Ceram. Soc.* 85(2002) 1921–1927.

[29] Z. Sun, H. Hashimoto, and W. Tian, Synthesis of the MAX Phases by Pulse Discharge Sintering. 718(2010) 704–718.

[30] B. Garcia-Diaz, L. Olson, C. Verst, R. Sindelar, E. Hoffman, B. Hauch, B. Maier and K. Sridharan MAX Phase Coatings for Accident Tolerant Nuclear Fuel. *Trans. Am. Nucl. Soc.*, vol. 110(2014) 994–996.

CHAPTER 2

LITERATURE REVIEW

2.1 Literature Review

MAX phases have gained significant attention from various research groups all around the globe. These phases possess superior properties of both metals and ceramics. Numerous researchers investigated the synthesis of MAX phases and studied its properties. The brief description of the efforts made by different researchers to study MAX phases are as follows:

In 2015, Anasori *et al.*[1] synthesized Mo_2TiAlC_2 ternary compound by pressure-less sintering. The powder mixture of Mo:Ti:Al:C was heated at 1600°C for 4h in the flowing argon atmosphere. The X-ray diffraction (XRD) pattern were refined by rietveld analysis to calculate the hexagonal lattice parameter a and c. High resolution transmission electron microscopy (HRTEM) confirmed the formation of a highly ordered Mo_2TiAlC_2 MAX phase in which Ti layer was sandwiched between two Mo layers and followed the Mo-Ti-Mo-Al-Mo-Ti-Mo stacking sequence.

In 2015, Anasori *et al.*[2] synthesized Mo_2TiAlC_2 and $Mo_2Ti_2AlC_3$ MAX phases via pressure-less sintering technique. The elemental ratio mMo:(3-m)Ti:1.1Al:2C was heated to 1600°C for 4h under the flowing argon atmosphere. The quantity of titanium was varied as m=1.5, 1.8, 2 or 2.2. The chemistries of Mo_2TiAlC_2 and $Mo_2Ti_2AlC_3$ were determined by X-ray photonelectron spectroscopy (XPS) to be $Mo_2TiAlC_{1.7}$ and $Mo_2Ti_{1.9}Al_{0.9}C_{2.5}$. The layering patterns as observed from high resolution scanning electron microscopy (HRSTEM) were Mo-Ti-Mo-Al-Mo-Ti-Mo for Mo_2TiAlC_2 and Mo-Ti-Ti-Mo-Al-Mo-Ti-Ti-Mo for $Mo_2Ti_2AlC_3$. As high density of states exists at Fermi level the obtained MAX phases exhibit metallic behaviour as per resistivity measurement over 300 to 10 K.

In 2015 Liu *et al.*[3] synthesized pure Ti_2AlN ternary nitride through thermal explosion (TE) of elemental powders Ti, Al, TiN. These were sintered at temperature ranges form 600-850°C in argon atmosphere for short holding time. XRD results revealed that, when the pellet was heated at 850°C, Ti_2AlN phase was present as pure phase along with intermetallic phases such as Ti_3Al, $TiAl_3$ and TiAl. During the formation of Ti_2AlN, exothermic reaction between Ti an Al powders occurred rapidly which led to the formation of molten TiAl. Further, TiN particles were dispersed into TiAl molten and precipitate of Ti_2AlN phase was formed during cooling process.

In 2015 Lapauw *et al.*[4] synthesized fine grained Ti_2SnC MAX phase by spark plasma sintering. The precursors Ti, Sn and C were sintered at temperature ranges from 1200-1400°C. However, the pure Ti_2SnC phase was formed at 1325°C along with Sn and TiC_X intermetallics present as minor phases which was confirmed by XRD. The elastic properties of Ti_2SnC compound formed were determined experimentally at room temperature. At room temperature,

the values of shear modulus, young modulus and possion ratio were found to be 83.9 GPa, 207.4 GPa and 0.2 respectively.

In 2015 Duan *et al.*[5] synthesized high purity bulk Cr_2AlC MAX phase using two-step sintering process. The elemental mixtures of Cr, Al and C were heated via pressure-less sintering in alumina crucible at 1400°C and coarse and fine grains of CrAlC powder were obtained. Further, these fine and coarse grain powder of Cr_2AlC were heat treated through spark plasma sintering at 1250°C in presence of argon environment under pressure of 50 MPa. It was observed in XRD patterns that the diffraction lines of the fine grained Cr_2AlC powder had broadened peak due to reduction in grain size after pressure-less sintering. The reduction diffraction lines of fine grained Cr_2AlC powder was observed after spark plasma sintering. The hardness of fine grained Cr_2AlC MAX phase was higher than coarse grained Cr_2AlC MAX phase. Thus, fine grained bulk Cr_2AlC ceramic exhibit anisotropic behaviour.

In 2016 Lapauw *et al.*[6] Investigated the formation of Zr_2AlC ternary compound by hot pressing. The starting materials ZrH_2, Al and C were heated at different temperatures 1475, 1525 and 1575°C. The atomic structure of Zr_2AlC was evaluated by high resolution transmission electron microscopy (HRTEM) which confirmed the 211-type atomic stacking. The pure phase Zr_2AlC was obtained at 1525°C and ZrC was present as secondary phase at 1475°C. The Vickers hardness of Zr_2AlC material was found to be 6.4±0.1GPa under the load of 30N.

In 2016 Lapauw *et al.*[7] synthesized two new Hf_4AlC_3 and Hf_3AlC_2 MAX phases in the Hf-Al-C system by hot pressing. The precursors HfH_2, Al and C were sintered at temperature range of 1500-1550°C in the vacuum atmosphere. The X-ray diffraction pattern revealed the formation of Hf_3AlC_2 and Hf_2AlC phases. It was noticed that the HfC phase was present as major phase along with some other intermetallic phase such as $HfAl_2$ Hf_2Al_3. High resolution transmission electron microscopy (HRTEM) confirmed the atomic structure in which the mixture of 211 and 312 stacking sequence were observed inside a particular grain which also included 512 stacking sequence.

In 2016 Lapauw *et al.*[8] synthesized Zr_3AlC_2 MAX phase by reactive hot pressing technique. The elemental powder of ZrH_2, Al, and C were heated at temperature of 1500°C. The phases such as Zr_3AlC_2, ZrC and $ZrAl_2$ obtained in X-ray diffraction (XRD) pattern were determined by rietveld refinement. The vickres hardness of obtained material was found to be 4.4 GPa. Hence, the produced Zr_3AlC_2 MAX phase has found potential applications for fuel cladding.

In 2016 Agne *et al.*[9] synthesized two Al-V_2AlC composites from elemental powders of Al:V:C as 9.8:2.0:1.0 and Al:V:C as 3.9 2.0:1.0. Elemental powders were heated to 1000°C for 0.5, 2.5 or 10 hours under Ar flow. The synthesis of V_2AlC composites was done by quenching below 1000°C. XRD and SEM results revealed the nature of AIR (aluminium rich) and VR (vanadium rich) phases, after quenching from 1000°C. Differential scanning calorimetry (DSC) analysis indicated the V_2AlC was unstable in liquid below 950°C. At 800°C, the Al and V_2AlC phases were found to be in equilibrium with both Al_3V and Al_4C_3.

In 2016 Shahin *et al.*[10] synthesized Ti_3AlC_2 ternary compound by mechanically induced combustion reaction (MSR). They studied the variation in ball milling time of initial materials (Ti, Al, C). The presence of Ti_3AlC_2 and TiC phases after the ball milling of 10h was revealed by X-ray diffraction. Scanning electron microscopy (SEM) confirmed the layered structure of Ti_3AlC_2 together with formation of TiC grains. However, rapid combustion reaction after 10h milling resulted in the formation of Ti_3AlC_2 and TiC.

In 2016 Madhu *et al.*[11] synthesized the Ti_3AlC_2 aluminium composites by friction stir processing (FSP) technique. The mixture of TiO_2+C was heated at different temperatures (633, 710, 951 °C) to form aluminium matrix composite. The X-ray diffraction pattern showed the formation of Ti_3AlC_2, Al, Ti_3Al and TiC phases at 633°C. Scanning electron microscopy analysis indicated the uniform distribution of particles. However, at 633°C the formation of TiC and Ti_3AlC_2 phases were confirmed by DSC. It was stated that due to particle refinement during FSP, activation energy of the reaction was lowered. This lowering of inactivation energy led to the formation of Ti_3AlC_2 and TiC phases.

In 2017 Kovalev *et al.*[12] synthesized $(Zr_{0.5}Ti_{0.5})AlC_2$ MAX phase by self-propagating method. The precursors Zr, Ti, Al C were heat treated at 1200°C in the presence of argon gas atmosphere. X-ray diffraction (XRD) and scanning electron microscopy (SEM) results revealed the presence of two phases: first was layered structure of $(Zr_{0.5}Ti_{0.5})AlC_2$ phase and second was carbide phase $(Zr_{0.5}Ti_{0.5})C_2$ has round grains.

1n 2017 Christoplous *et al.*[13] investigated the intrinsic defects in M_3AlC_2 (M=V, Ti, Ta, Zr) MAX phases via density functional theoretical calculations. Among the intrinsic disordered mechanism, Frenkel defect and Antisite defects were more dominant defects reactions. DFT calculations revealed that Ti_3AlC_2 MAX phase has high intrinsic defects energy as compared to other MAX phases. Therefore, Ti_3AlC_2 MAX phase has greater radiation tolerance. It was concluded that the concentration of point defect affects the lattice stability and the ability of MAX phase to amorphize below radiation environment.

In 2017 Rasid *et al.*[14] synthesized Ti_3C_2 MXene from Ti_3AlC_2 MAX phase after chemical etching of 20 h. The Ti_3AlC_2 ternary compound was prepared by low cost pressure-less sintering method at 1350°C. XRD results revealed the presence of four phases Ti_3AlC_2, TiO_2 and TiC before sintering. The same four phases were observed after sintering as observed in XRD pattern. However, it was observed that after chemical etching with hydrofluoric acid, the Ti_3AlC_2 phase has fully diminished. Scanning electron microscopy (SEM) images showed the clusters of Al_2O_3 and graphite which confirmed the formation of Ti_3C_2 MXene layer. Hence, the 2D Ti_3C_2 MXene was successfully synthesized by this method.

In 2018 Hamm *et al.* [15] synthesized bulk V_2AlC and Mn-doped $(V_{1-x}Mn_x)_2AlC$ via microwave heating and spark plasma sintering. The elemental mixture of V, Mn, Al and C was firstly heated in microwave for 30 min and then for densification sample was heated at temperature 1000°C. X-ray diffraction pattern indicated that V_2AlC obtained at x= 0.5 single phase, $(V_{1-x}Mn_x)_2AlC$ single phase was obtained at x=0.1 and 0.15. By performing electron microscopy at various length scales, the level of Mn doping was determined. Therefore, the average doping level of Mn was 2% analogous to $(V_{0.96\pm0.02,}Mn_{0.04\pm0.02})_2AlC$. The Mn doped MAX phases showed the metallic character which was revealed by electronic property. Hence, the Mn doped MAX phase with chemical composition $(V_{0.96}Mn_{0.04})_2AlC$ showed the combination of Pauli and Langevin paramagnetism.

In 2018 Mane *et al*. [16] synthesized Ti_3GeC_2 MAX phase powder by pressure-less sintering technique. The elemental mixture of Ti, Ge and C were sintered at temperature range of 1200 to 1500°C under the flowing Ar. It was observed that the formation of pure Ti_3GeC_2 phase, when sintered at different temperatures (1200, 1400 and 1500°C) was confirmed by the X-ray diffraction (XRD) results. It was found that the powder of Ti_3GeC_2 revealed the lack of densification during sintering process and slow grain growth as compared to other MAX phases.

In 2018 Jankowiak *et al.*[17] synthesized Nb_4AlC_3 MAX phase via in-situ hot pressing reaction of initial materials Nb, Al, NbC, which were heated upto 1735°C under the argon environment. The pure Nb_4AlC_3 phase was obtained at 1735°C which was confirmed by DTA results. It was also observed from the DTA that porosity of the sample decreases along with increase in densification as the temperature increases. XRD pattern confirmed the formation of $NbAl_3$ along with intermetallics such as Nb_2Al and Nb_3Al around 1000°C. The obtained material had average grain size of 7-10 µm. Nb_4AlC_3 phase contained 13% alumina contents in comparison to 50% contained in $NbAl_3$ and their oxidation performance was evaluated at 1100°C.

In 2018 Christoplous *et al.*[18] investigated intrinsic defects in Ti_3AC (A=Al, Si, Ga, Ge, In, Sn) MAX phases by density functional theory. Among the intrinsic disordered mechanism, it was calculated that Frenkel defect was more dominating . DFT calculations revealed that Ti_3SnC_2 MAX phase has high intrinsic defects energy as compared to other MAX phases. Therefore, Ti_3AlC_2 MAX phase has high tolerance. On the basis of elastic properties of Ti_3AC_2 ternary compound, it was observed that Ti_3SiC_2 was the hard and Ti_3SnC_2 was soft MAX phases. It was concluded that Ti_3AC_2 phases are non-central forces and brittle in nature. On the other hand, Ti_3SiC_2 was elastically more anisotropic and Ti_3AlC_2 was isotropic in nature.

In 2018 Akhlaghi *et al.*[19] synthesized Ti_3AlC_2 ternary compound through wave propagation and thermal explosion of elemental powders Ti, Al and C. These powders undergo combustion reaction in reaction chamber and the combustion reaction was carried out in tube furnace around 1000°C. XRD results revealed the presence of Ti_3AlC_2 phase as major phase together with formation of TiC as by product. Scanning electron microscopy (SEM) micrographs demonstrate the dark-colored layered microstructure of Ti_3AlC_2 phase and light-colored spherical phase of TiC by product and Ti_3AlC_2 had thicker grains. Layered Ti_3AlC_2 phase contained higher Al content as compared to spherical phases was verified by energy dispersive spectroscopy.

In 2018 Wang *et al.*[20] synthesized $Ti_3(Si,Al)C_2$ intermetallic compound through high energy consumption synthesis process. The elemental powder of Ti, Al, Si and C were compacted by conventional die pressing method under the pressure of 150 MPa. These powder mixtures were heated in vacuum furnace at 1300°C. The produced porous $Ti_3(Si,Al)C_2$ quaternary compound exhibit good pore structure property and had average pore size of 4.4 µm. The synthesized porous $Ti_3(Si,Al)C_2$ quaternary compound was characterized by a substitution solid solution based on Ti_3SiC_2 with a percentage of Si replaced by Al atoms.

References

[1] B. Anasori, J. Halim, J. Lu, C. A. Voigt, L. Hultman and M. W. Barsoum, Mo_2TiAlC_2: A new ordered layered ternary carbide. *Scr. Mater.* 101(2015) 5–7.

[2] B. Anasori, J. Halim, J. Lu, C. A. Vigot, L. Hultman and M. W. Barsoum Experimental and theoretical characterization of ordered MAX phases Mo_2TiAlC_2 and $Mo2Ti_2AlC_3$. *J. Appl. Phys.*118(2015) 094304.

[3] Y. Liu, L. Zhang, W. Xiao, L. Zhang, Y. Pu and S. Guo Rapid synthesis of Ti_2AlN ceramic via thermal explosion. *Mater. Lett.* 149(2015) 5–7.

[4] T. Lapauw, K. Vanmeensel, K. Lambrinou and J. Vleugels, Rapid synthesis and elastic properties of fine-grained Ti_2SnC produced by spark plasma sintering. *J. Alloys Compd.* 631(2015) 1–15.

[5] X. Duan, L. Shen, D. Jia, Y. Zhou, S. V. Zwaag and W. G. Sloof, Synthesis of high-purity, isotropic or textured Cr_2AlC bulk ceramics by spark plasma sintering of pressure-less sintered powders. *J. Eur. Ceram. Soc.* 35(2015) 1393–1400.

[6] T. Lapauw, K. Lambrinou, T. Cabioc'h, J.Halim , J. Lu, A. Pesach, O. Rivin, O.Ozeri, E. N. Capsi, L. Hultman, P. Eklund, J. Rosen, M.W. Barsoum and J. Vleugels, Synthesis of the new MAX phase Zr_2AlC. *J. Eur. Ceram. Soc.* 36(2016) 1847–1853.

[7] T. Lapauw, B. Tunca, T. Cabioc'h, O. A. Persson, K. Lambrinou and J. Vleugels, Synthesis of MAX Phases in the Hf−Al−C System, *J. Am. Chem. Soc*. 55(2016) 10922−10927.

[8] T. Lapauw, J.Halim, J. Lu, T. Cabioc'h, L. Hultman, M.W. Barsoum, K. Lambrinou and J. Vleugels, Synthesis of the novel Zr_3AlC_2 MAX phase. *J. Eur. Ceram. Soc.* 36(2016) 943–947.

[9] M. T. Agne, M. Radovic, G. W. Bentzel and M. W. Barsoum, Stability of V_2AlC with Al in 800-1000 °C temperature range and in situ synthesis of V_2AlC/Al composites. *J. Alloys Compd.*, 666(2016) 279–286.

[10] N. Shahin, S. Kazemi and A. Heidarpour, Mechanochemical synthesis mechanism of Ti_3AlC_2 MAX phase from elemental powders of Ti, Al and C, *Adv. Powder Technol.* 27(2016) 1775–1780.

[11] H. C. Madhu and S. V. Kailas, In-Situ Aluminothermal Reduction Synthesis of Ti_3AlC_2 Aluminium Composite by Friction Stir Processing. *Procedia Manuf.* 7(2017) 157–162.

[12] D. Y. Kovalev, M. A. Luginina, S. G. Vadchenko, S. V. Konovalikhin, A. E. Sychev and A. S. Shchukin, Synthesis of a new MAX phase in the Ti–Zr–Al–C system. *Mendeleev Commun.* 27(2017) 59–60.

[13] S. R. G. Christopoulos, N. Kelaidis, and A. Chroneos, Defect processes of M_3AlC_2 (M = V, Zr, Ta, Ti) MAX phases. *Solid State Commun.* 261(2017) 54–56.

[14] Z. A. M. Rasid, M. F. Omar, M. F. M. Nazeri, M. A. A. A'ziz and M. Szota, Low Cost Synthesis Method of Two-Dimensional Titanium Carbide MXene. *IOP Conf. Ser. Mater. Sci. Eng.* 209(2017) 012001.

[15] C. M. Hamm, M. Durrschnabel, L. M ona-Luna, R. Salikhov, D. Spoddig, M. Farle, U. Wiedwald and C. S. Birkel, Structural, magnetic and electrical transport properties of non-conventionally prepared MAX phases V_2AlC and $(V/Mn)_2AlC$, *Mater. Chem. Front.* 2018.

[16] R. B. Mane, A. Haribabu and B. B. Panigrahi, Synthesis and sintering of Ti_3GeC_2 MAX phase powders. *Ceram. Int.* 44(2018) 890–893.

[17] A. Julian-Jankowiak and P. Sallot, Microstructure and Mechanical properties of

Nb_4AlC_3 MAX phase synthesized by reactive Hot Pressing. *Ceram. Int.* 2018.

[18] S. R. G. Christopoulos, P. P. Filippatos, M. A. Hadi, N. Kelaidis, M. E. Fitzpatrick and A. Chroneos, Intrinsic defect processes and elastic properties of Ti_3AC_2(A = Al, Si, Ga, Ge, In, Sn) MAX phases. *J. Appl. Phys.* 123(2013) 025103.

[19] M. Akhlaghi, S. A. Tayebifard, E. Salahi, M. Shahedi Asl and G. Schmidt, Self-propagating high-temperature synthesis of Ti_3AlC_2 MAX phase from mechanically-activated Ti/Al/graphite powder mixture. *Ceram. Int.* 44(2018) 9671–9678.

[20] Z. Wang, H. Zhang, X. Liu, Y. Jiang, H. Gao and Y. He, Reactive synthesis of porous nanolaminate $Ti_3(Si,Al)C_2$ intermetallic compound. *Mater. Chem. Phys.* 208(2018) 85–90.

CHAPTER 3

MATERIALS & METHODS

3.1 Raw Materials

The initial precursor used for the synthesis of Mo_2TiAlC_2 MAX phase were molybdenum (*Sigma Aldrich*), titanium carbide (*Sigma Aldrich*), aluminium (*SD Fine Chem Limited*) and graphite (*Sigma Aldrich*). All chemicals were used without any further purification.

3.2 Methodology

The experiments were categorized in two series based on titanium source used for the synthesis of Mo_2TiAlC_2. The experimental details are presented in the flow chart (Fig. 3.1) given below**.**

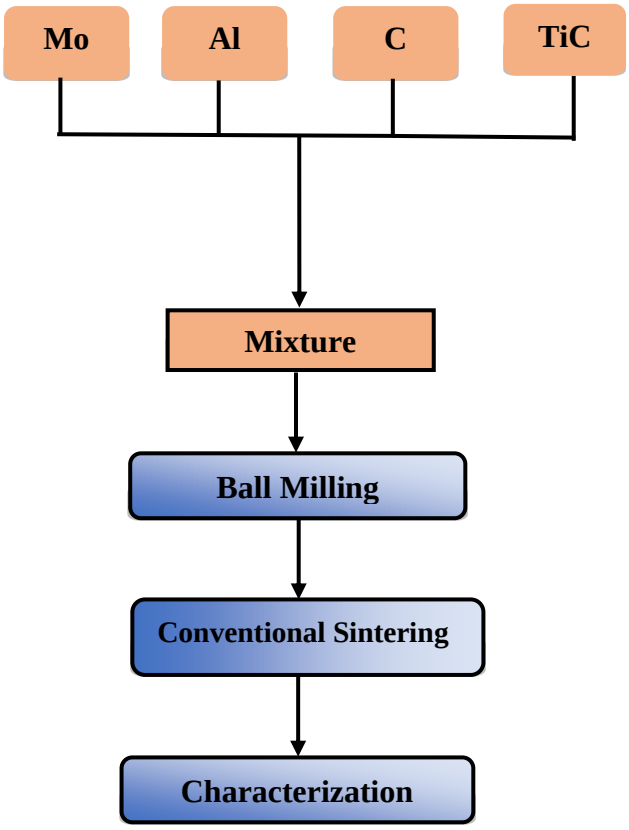

Figure 3.1: Flow chart for the synthesis of Mo_2TiAlC_2.

In both series, the powders were dry milled in a tungsten carbide jar (100 ml) for 1 hr at 200 rpm in argon environment using *RESTCHPM-100* ball mill. The charge ratio was 15:1 for the milling process and tungsten carbides balls (10 mm Dia) were used for milling purpose. Afterwards, the powder was cold pressed by applying 200 MPa pressure in a hydraulic press (*CAP-15T, Pciss*). The pellets of ~ 10 mm diameter and ~ 3 mm thickness were prepared. Further, the prepared pellets were sintered in a tubular furnace (*LTF 18/75/300, Lenton Thermal Design)* at 5 °C/min heating rate. All the experiments were performed in high purity argon. The initial composition and sample naming of ball milled samples in series is presented in Table 3.1. Further, the ball milled samples of series was sintered at various temperatures i.e.

1400 °C, 1500 °C and 1600 °C. Also, the dwell time was varied to obtain Mo_2TiAlC_2 MAX phase. Figure 3.2 shows the schematic representation of the synthesis process of series.

After sintering at desired temperature, the pellets were cooled to room temperature in the furnace itself with continuous argon flow. The sintered samples ID of series is presented in Table 3.2 respectively.

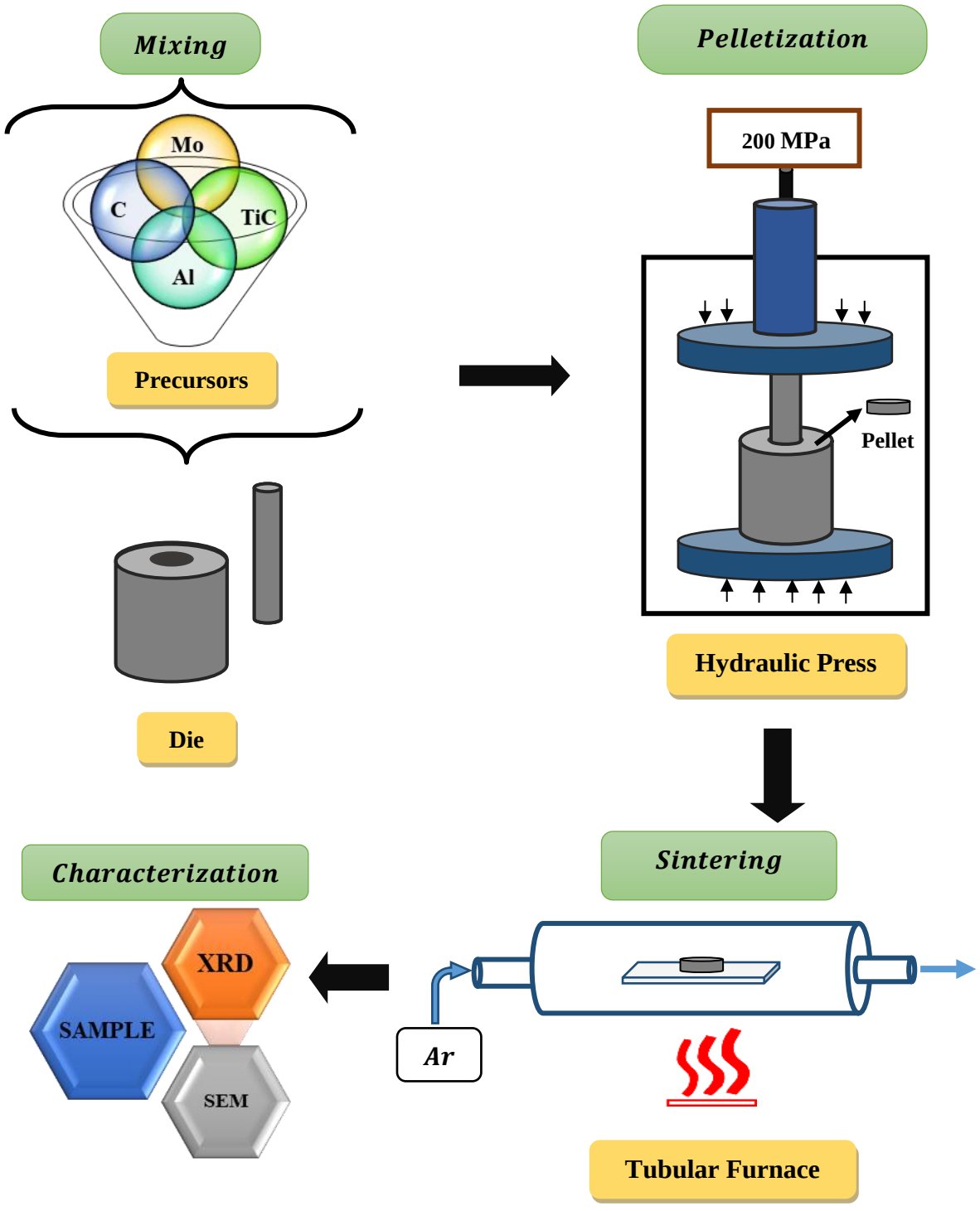

Figure 3.2: Schematic representation of synthesis for Mo_2TiAlC_2 MAX phase.

Table 3.1 The initial composition and sample ID of all samples in series.

SERIES				
Sample	**Precursors**			
ID	**Mo**	**TiC**	**Al**	**C**
MAC1			1	
MAC2			1.1	
MAC3	2	2	1.2	1
MAC4			1.3	
MAC5			1.4	

Table 3.2 Sintered samples ID of series.

S.No.	Sample ID	Temperatures (°C)	Dwell Time (Hrs.)
1	14-MAC1	1400	1
2	14-MAC2		
3	14-MAC3		
4	14-MAC4		
5	14-MAC5		
6	15-MAC1	1500	
7	15-MAC2		
8	15-MAC3		
9	15-MAC4		
10	15-MAC5		
11	16-MAC1	1600	
12	16-MAC2		
13	16-MAC3		
14	16-MAC4		
15	16-MAC5		
16	14-MAC1-4	1400	4
17	14-MAC2-4		
18	14-MAC3-4		
19	14-MAC4-4		
20	14-MAC5-4		

21	15-MAC1-4	1500	4
22	15-MAC2-4		
23	15-MAC3-4		
24	15-MAC4-4		
25	15-MAC5-4		

3.3 Characterizations

3.3.1 X-ray Diffraction (XRD)

XRD diffraction analysis of prepared samples were done by *PANalytical Xpert Pro* XRD diffractometer having Cu-Kα radiation λ= 1.5418 Å to determine the corresponding peaks of MAX phase. The applied voltage was kept at 45 kV and current at 40 mA. All synthesized samples were placed in a sample holder and scanned in defined range of 2θ from 10° - 90° with step size of 0.0131. The corresponding peaks of all samples were identified by using *X'Pert Highscore* Plus software with reference International Centre for Diffraction Data (ICCD) card.

3.3.2 Scanning Electron Microscopy (SEM)

Scanning electron microscopy (SEM) is generally used for the characterization of surface morphology of the prepared samples. In this technique, the beam of electrons generated in a vacuum and that beam is collimated by electromagnetic lenses, fixated by an objective lens and scanned over the surface of the sample. In SEM, samples were analysed by placing them on the C-tape. The samples were analysed with JEOL (JSM-IT100). EDS analysed the chemical composition of the sample.

CHAPTER 4

RESULTS & DISCUSSION

4.1. X-Ray Diffraction (XRD) Analysis

Fig 4.1 shows the XRD patterns of MAC1- MAC5 samples ball milled for 1hr at a 200 rpm. In these samples the content of aluminium is varied from the stoichiometry ratio to higher side. Several researchers also varied aluminium concentration to synthesis pure MAX phases. Similar variation of aluminium in Ti-Al-C MAX phase was done by Hendaoui *et al.* [1] to get pure phase. To obtain high purity Ti_3SiC_2 MAX phase the variation in aluminium was also done by Jiaoqun *et al.* [2]. However, there is no significant variation in the XRD patterns of ball milled samples is observed with increase in aluminium concentration. The XRD patterns almost remain the same with increase in aluminium content. The volume fraction of the prepared samples is calculated by using Gaussian curve fitting. Table 4.1 shows the volume fraction of the distinct phases present in the XRD patterns.

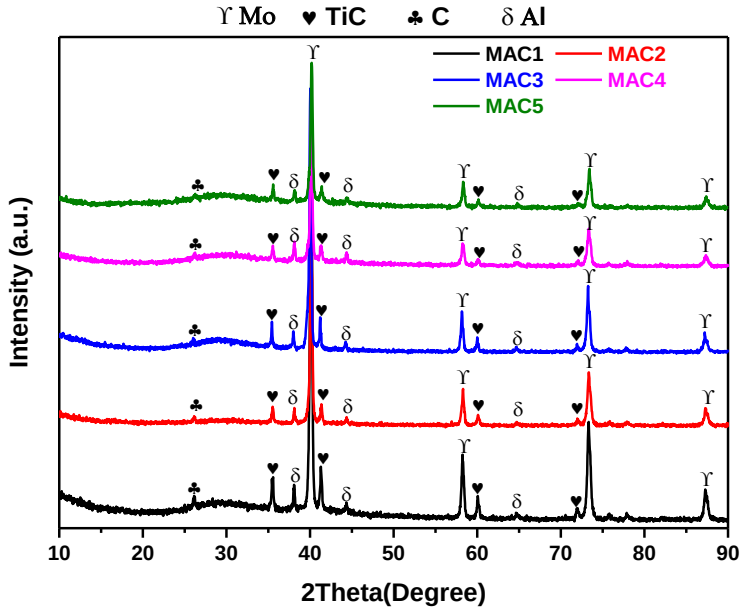

Figure 4.1 XRD pattern of ball milled MAC1-MAC5 samples.

It can be observed from the table 4.1 that with increase in aluminium content, the volume fractions of aluminium phase increased from 3.70 to 5.69. However, the volume fractions of molybdenum (Mo), graphite (C) and titanium carbide (TiC) phases decreased. In these samples Mo exists as major phase, whereas other phases like TiC, C, and Al as secondary phases.

Further, to synthesis Mo_2TiAlC_2 phase the samples (14-MAC1 – 14-MAC5) were sintered at 1400°C for one hour of dwell time. Fig. 4.2 present the XRD of the samples sintered at 1400°C. In this figure, the formation of multiphase alloys i.e. Mo_3Al_2C, $MoTiC_2$, $MoTiAl_6$

and Mo_2C was observed. Formation of Mo_2TiAlC_2 does not occur. The volume fraction of all the phases present in the samples sintered at 1400°C are presented in table 4.2. It is observed from the table that the volume fraction of all the phases remains same. Also, no significant impact of aluminium content is observed in these samples. Moreover, this indicates that the reaction requires more energy for the formation of Mo_2TiAlC_2 phase. So, the sintering temperature is increased to 1500°C and dwell time remains the same.

Table 4.1 Volume fractions of distinct phases present in samples MAC1 – MAC5.

Sample ID	Volume Fraction (%)			
	Al	Mo	TiC	C
MAC1	3.70	85.28	10.01	1.22
MAC2	3.18	84.56	11.04	1.15
MAC3	4.82	84.83	9.25	1.09
MAC4	5.98	84.60	7.68	1.40
MAC5	5.69	84.56	7.23	1.40

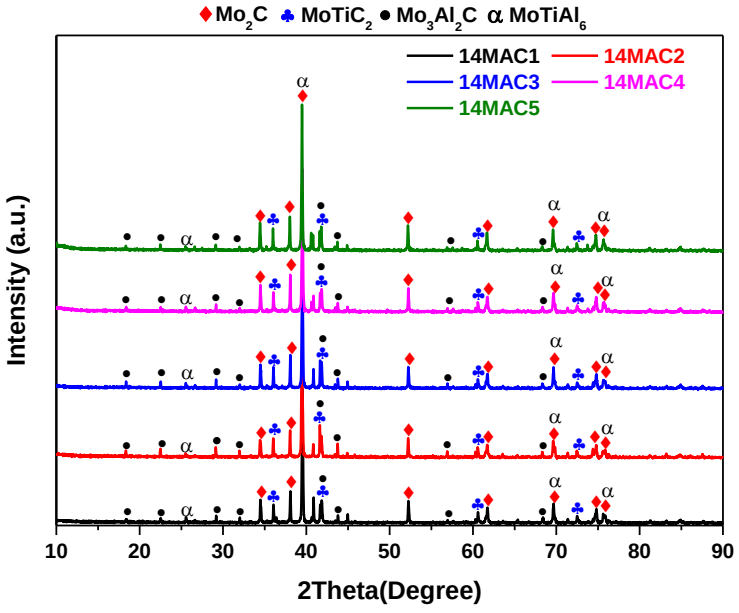

Figure 4.2 XRD pattern of 14MAC1- 14MAC5 samples sintered at 1400°C for 1 hr.

Table 4.2 Volume fractions of distinct phases in 14MAC1 - 14MAC5 samples sintered at 1400°C.

Sample ID	Volume Fraction (%)			
	Mo_2C	Mo_3Al_2C	$MoTiC_2$	$MoTiAl_6$
14MAC1	81.47	8.43	11.91	46.38
14MAC2	78.80	10.15	11.51	44.50
14MAC3	76.16	9.95	10.95	44.18
14MAC4	78.58	7.59	10.67	45.27
14MAC5	78.89	6.92	9.76	55.05

Fig. 4.3 represents the XRD pattern of the samples (15-MAC1 – 15MAC5) sintered at 1500°C. In this case, Mo and Mo_3Al_2C phases are found to be the major phase in all the samples. Also, no peak associated with Mo_2TiAlC_2 phase is observed. The volume fraction (table 4.3) of Mo_3Al_2C increased when the samples sintered at 1500°C as compared to 1400°C. However, the formation of Mo_2TiAlC_2 phase is not observed in 15-MAC1 – 15MAC5 samples. Therefore, the reaction temperature was further increased to 1600°C for the formation of Mo_2TiAlC_2 phase.

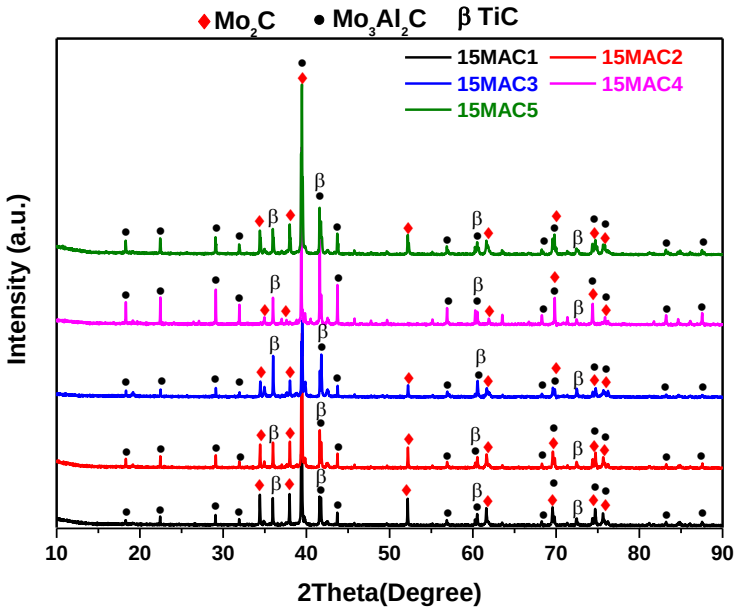

Figure 4.3 XRD pattern of 15MAC1 – 15MAC5 samples sintered at 1500°C.

Table 4.3 Volume fractions of distinct phases in 15MAC1 – 15MAC5 samples sintered at 1500°C.

Sample ID	Volume Fraction (%)		
	Mo_2C	Mo_3Al_2C	TiC
15MAC1	61.38	26.57	15.26
15MAC2	57.06	25.66	13.96
15MAC3	46.70	34.24	34.88
15MAC4	44.52	36.47	24.61
15MAC5	50.84	36.39	26.40

Fig. 4.4 represents the XRD results of samples (16-MAC1 – 16-MAC5) sintered at 1600°C for 1 hr. The presence of Mo_2C as major phase and TiC as secondary phases is observed in the XRD patterns. The volume fractions of observed phases are summarized in table 4.4. As aluminium increases from 0 to 40 mol%, the volume fractions of Mo_2C increased gradually, whereas the volume fraction of TiC decreased. However, the formation of Mo_2TiAlC_2 is not observed in all the samples sintered at 1400°C, 1500°C and 1600°C. So, in the next step the dwell time is varied to 4 hours to investigate the formation of Mo_2TiAlC_2 phase.

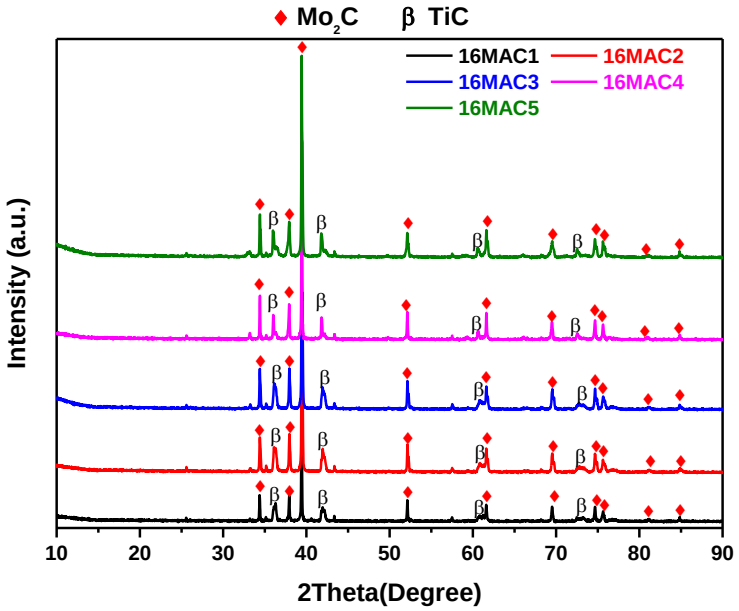

Figure 4.4 XRD pattern of 16MAC1 – 16MAC5 samples sintered at 1600°C.

Table 4.4 Volume fractions of distinct phases in 16MAC1 – 16MAC5 samples sintered at 1500°C.

Sample ID	Volume Fraction (%)	
	Mo_2C	TiC
16MAC1	50.19	26.57
16MAC2	63.84	25.66
16MAC3	68.51	34.24
16MAC4	74.87	36.47
16MAC5	82.91	36.39

Fig. 4.5 shows the XRD patterns of the samples (14MAC1-4 – 14MAC5-4) sintered at 1400°C for 4 hours of dwell time. XRD patterns depicted the presence of four phases i.e. Mo, C, TiC and Mo_3Al. In this case, Mo exists as major phase and other phases C, TiC, and Mo_3Al as secondary phases. Based on the XRD patterns volume fractions of observed phases were calculated and listed in table 4.5.

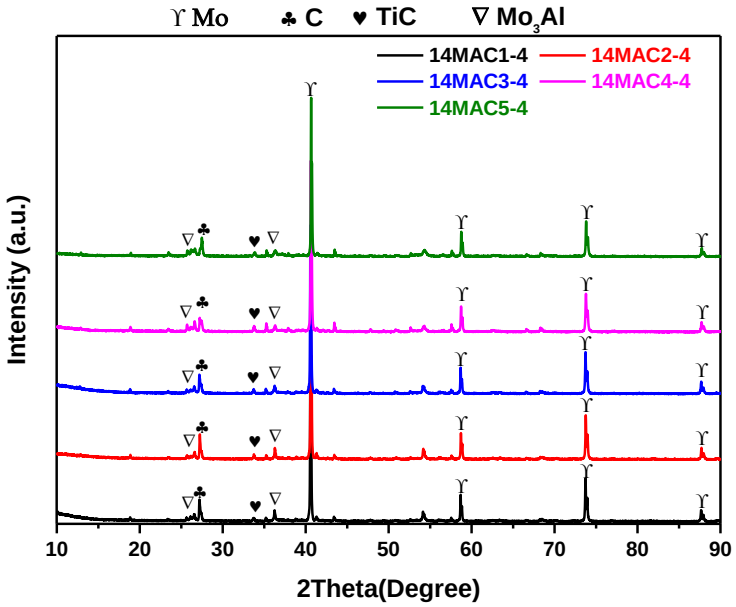

Figure 4.5 XRD pattern of 14MAC1-4 – 14MAC5-4 samples sintered at 1400°C for 4 hrs.

Comparable results are obtained when the samples (15MAC1-4 – 15MAC5-4) were sintered at 1500°C for fours of dwell time. The XRD patterns results of sintered 15MAC1-4 – 15MAC5-4 samples are shown in Fig. 4.6 and the volume fraction calculated for distinct

phases. It is observed from the XRD pattern that Mo is present as main phase, while C and Mo_2C as secondary phases and some of the peaks were unidentified.

Table 4.5 Volume fractions of distinct phases in 14MAC1-4 – 14MAC5-4 samples sintered at 1400°C for 4 hours.

Sample ID	Volume Fraction (%)			
	Mo	C	Mo_3Al	TiC
14MAC1-4	87.49	4.14	5.98	2.28
14MAC2-4	87.81	4.27	5.51	2.39
14MAC3-4	86.18	4.64	6.67	2.45
14MAC4-4	84.89	4.67	7.87	2.60
14MAC5-4	82.68	4.93	7.96	2.93

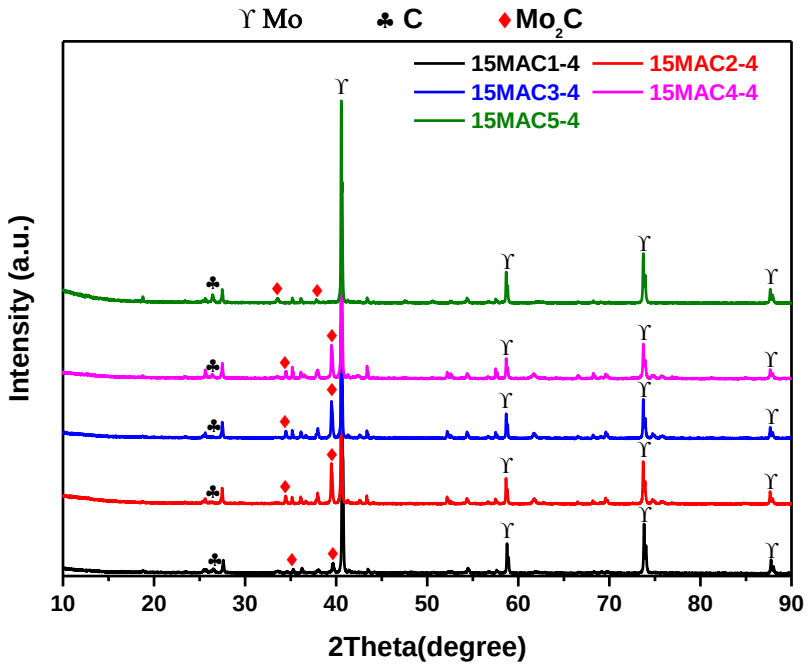

Figure 4.6 XRD pattern of 15MAC1-4 – 15MAC5-4 samples sintered at 1500°C for 4 hours.

The experimental conditions seem to be not appropriate for the formation of Mo_2TiAlC_2 MAX phases. The formation of a material/alloy requires choice of suitable initial precursor. So, in the next series pure titanium is used as titanium source for the synthesis of MAX phase.

Table 4.6 Volume fractions of distinct phases in 15MAC1-4 – 15MAC5-4 samples sintered at 1500°C for 4 hours.

Sample ID	Volume Fraction (%)		
	Mo_2C	Mo	C
15MAC1-4	19.58	73.63	6.53
15MAC2-4	25.72	67.59	6.68
15MAC3-4	23.22	69.43	7.34
15MAC4-4	27.33	65.84	6.82
15MAC5-4	31.92	60.89	7.19

4.2 Scanning Electron Microscopy (SEM)

Fig 4.7 shows the micrographs of samples 15MAC3-4 sintered at 1500°C for one hour. The microstructure analysis revealed the presence of nano-laminated structure, which corresponds to the MAX phase. The specific feature of the MAX phase is observed in all the images.

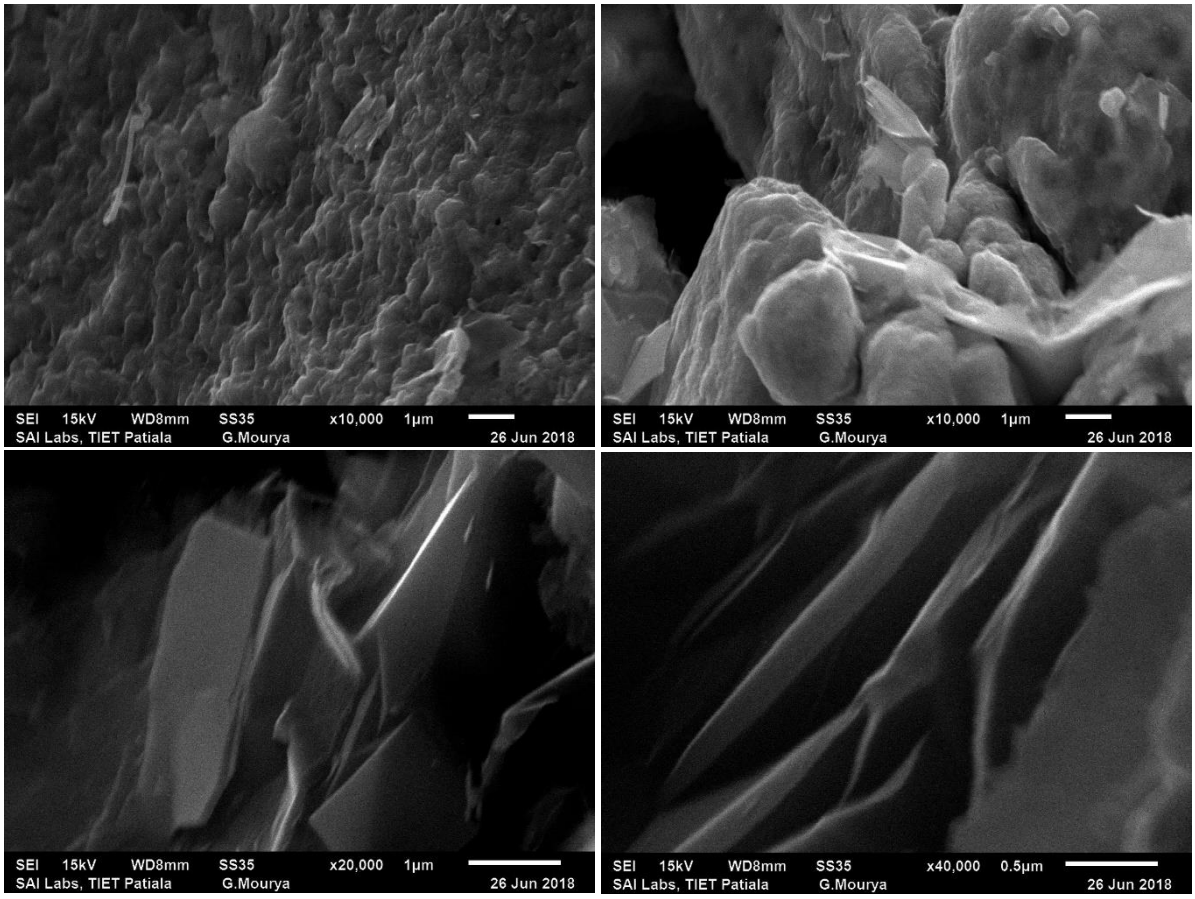

Figure 4.7 SEM images of 15MAC3-4 sample sintered at 1500°C.

Also, EDS mapping was done to examine the distribution of the elements and to identify the elemental composition of all the element. Fig. 4.8 - 4.9 shows the EDS elemental composition and mapping of 15MAC3-4 sample.

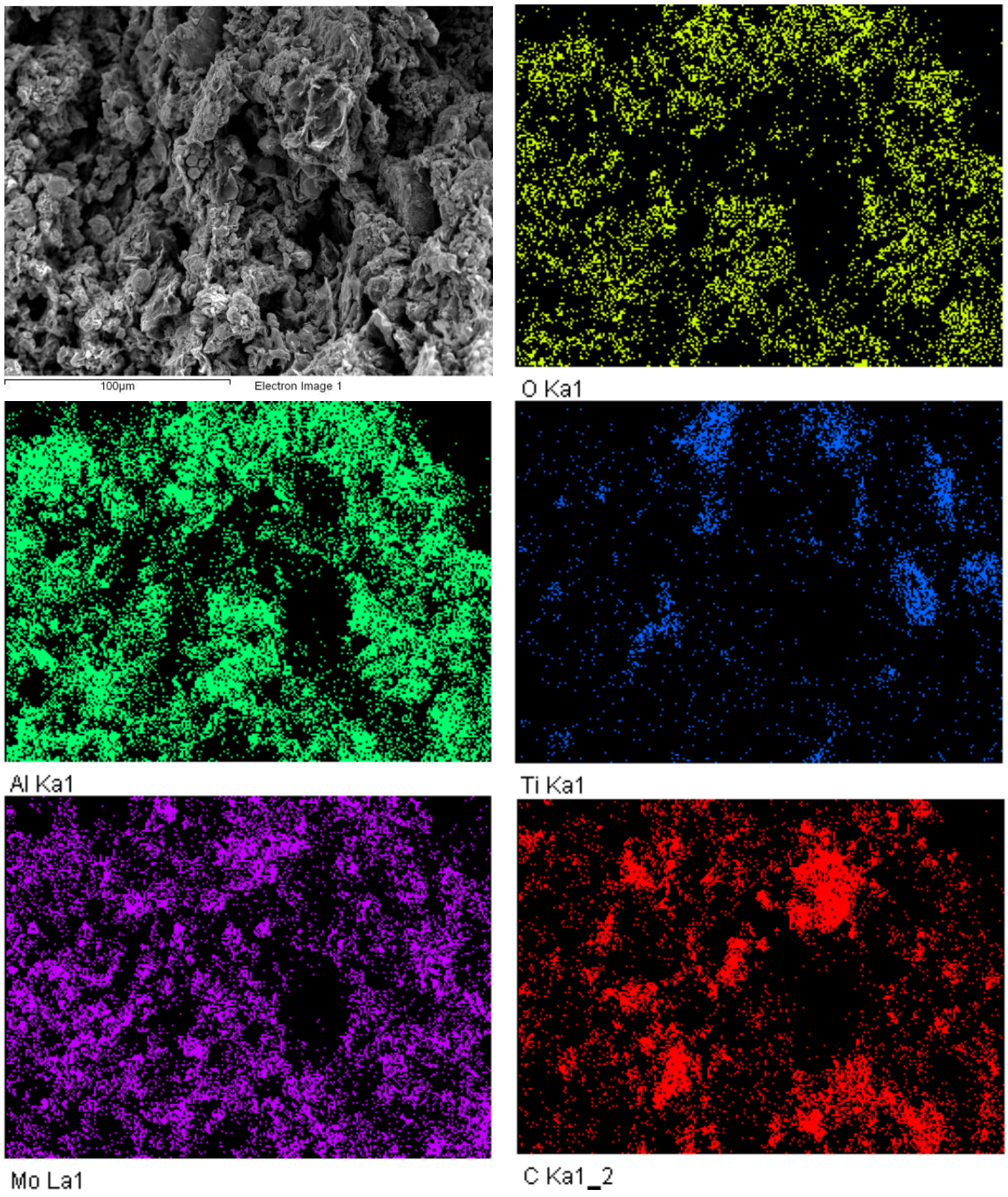

Figure 4.8 EDS mapping of 15MAC3- 4 sample sintered at 1500°C.

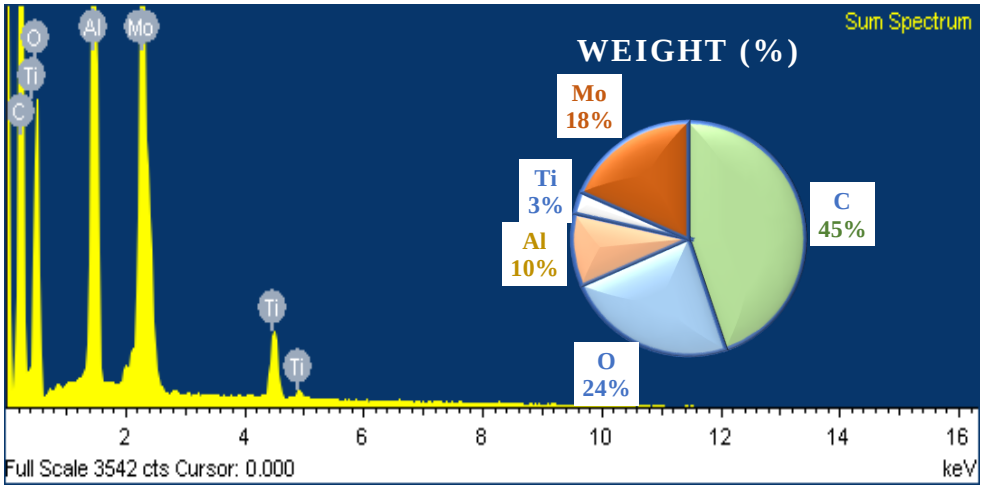

Figure 4.9 Elemental composition of 15MAC3-4 sample sintered at 1500°C.

References

[1] A. Hendaoui, D. Vrel, A. Amara, A. Benaldjia and P. Langlois, Ti-Al-C MAX phases by aluminothermic reduction process. *Int. J. Self-Propagating High-Temperature Synth.* 17(2008) 125–128.

[2] J. Zhu and B. Mei, Fabrication of high-purity Ti_3SiC_2 by spark plasma sintering (SPS) of elemental powders. *J. Mater. Sci.* 22(2003) 889–890.

[3] B. Anasori, Y. Xie, M. Beidaghi, J. Lu, B. C. Hosler, L. Hultman, P. R. C. Kent, Y. Gogotsi, and M. W. Barsoum. Two-Dimensional, Ordered, Double Transition Metals Carbides (MXenes). *ACS Nano*. 9(2015) 9507–9516.

CHAPTER 5

CONCLUSION & FUTURE SCOPE

5.1. Conclusion and Future Scope

The Mo_2TiAlC_2 MAX phase was successfully synthesized by conventional sintering technique. In series I, titanium carbide was used as the source of titanium, while in series II pure titanium was used. The XRD pattern revealed the peaks of Mo_2TiAlC_2 MAX phase in the case of pure titanium when heated at various temperatures *i.e.* 1400 °C, 1500 °C and 1600 °C for one - hour holding time. The surface morphology of as-prepared samples revealed that layers started forming at 1500°C and complete layers are formed with kink bandings at 1600°C.

To obtain a pure MAX phase the optimization in technical parameters like ball to powder ratio, variation in sintering temperatures as well as in dwell time could be done. Concentration of titanium could be varied instead of variation in aluminium. Moreover, electrical properties of obtained MAX phase could be studied. In addition to this, etching of A layer element from MAX phase could be done to obtain a corresponding MXene. Furthermore, the potential application in electrochemistry of prepared MXenes could be studied.